

Velocity gradients statistics along particle trajectories in turbulent flows: the refined similarity hypothesis in the Lagrangian frame

Roberto Benzi,¹ Luca Biferale,¹ Enrico Calzavarini,² Detlef Lohse,³ and Federico Toschi⁴

(International Collaboration for Turbulence Research)

¹*Dept. Physics and INFN, University of Tor Vergata,
Via della Ricerca Scientifica 1, 00133 Rome, Italy.*

²*Lab. de Physique, École Normale Supérieure de Lyon,
CNRS UMR5672, 46 Allée d'Italie, 69007 Lyon, France.*

³*Dept. of Science and Technology, Impact Institute, and Burgers Center,
University of Twente, 7500 AE Enschede, The Netherlands.*

⁴*Dept. Physics and Dept. Mathematics & Computer Science,
Eindhoven University of Technology, P.O. Box 513, 5600 MB Eindhoven, The Netherlands.*

(Dated: October 30, 2018)

We present an investigation of the statistics of velocity gradient related quantities, in particular energy dissipation rate and enstrophy, along the trajectories of fluid tracers and of heavy/light particles advected by a homogeneous and isotropic turbulent flow. The Refined Similarity Hypothesis (RSH) proposed by Kolmogorov and Oboukhov in 1962 is rephrased in the Lagrangian context and then tested along the particle trajectories. The study is performed on state-of-the-art numerical data resulting from numerical simulations up to $Re_\lambda \sim 400$ with 2048^3 collocation points. When particles have small inertia, we show that the Lagrangian formulation of the RSH is well verified for time lags larger than the typical response time τ_p of the particle. In contrast, in the large inertia limit when the particle response time approaches the integral-time-scale of the flow, particles behave nearly ballistic, and the Eulerian formulation of RSH holds in the inertial-range.

PACS numbers: 47.27.-i, 47.10.-g

I. INTRODUCTION

One of the most prominent features of turbulent flows is the strong variation present in the energy dissipation field, a phenomenon called intermittency [1]. In an attempt to describe quantitatively intermittent fluctuations in the inertial range of turbulence, Kolmogorov and Oboukhov in 1962 [2, 3] proposed a general relation linking velocity fluctuations, measured at a given spatial increment $\delta_r u = u(x+r, t) - u(x, t)$, with the statistical properties of the coarse grained energy dissipation, $\varepsilon_r = r^{-3} \int_{\Lambda(r)} \varepsilon(\mathbf{x}, t) d^3x$ averaged over a volume, $\Lambda(r)$, of typical linear size r :

$$\delta_r u \sim r^{1/3} \varepsilon_r^{1/3}, \quad (1)$$

where \sim means “scales as” or “equal in law”. Equation (1) is known as the Refined (Kolmogorov) Similarity Hypothesis (RSH) and it is considered to be one of the most remarkable relations between turbulent velocity fluctuations: Many efforts in the last decades have been devoted to its validation ([4, 5, 6]). The importance of RSH cannot be underestimated: it bridges inertial-range properties with small-scale properties, supporting the existence of an energy cascade mechanism, statistically local in space. So far, a rather strong evidence supports the validity of the RSH in the Eulerian frame (i.e. the laboratory frame). On the other hand, no investigation has been reported in the literature on the validity of RSH in the Lagrangian frame (i.e. along fluid particle trajectories). The main difficulty in studying RSH in a moving

reference frame stems from the necessity to make multi-point measurements along particle trajectories in order to calculate the stress tensor. As a result, no experimental measurements along particle trajectories of velocity gradients exists for time long enough to be able to evaluate temporal correlations. Also numerical experiments are very demanding, requiring refined computations of velocity differences along particle trajectories. This is usually implemented by computing the velocity gradients matrix in Fourier space, then transforming it to physical space by (inverse) Fast Fourier Transform, and performing off-grid interpolations of the gradients at the particle positions. Here we report the first of such measurements using high-resolution Direct Numerical Simulations (DNS) investigations. We also note that when the particles transported in a turbulent environment have non-negligible size or mass, i.e. they are inertial particles, their trajectories becomes strongly sensitive to the statistical and topological properties of the advecting flow ([7, 8, 9, 10]). The possible validity of Lagrangian RSH in this context is far from being trivial and may shed new light on the physics of particulate transport in turbulent flows: an ubiquitous phenomena in nature and in industrial applications alike.

In the present study we will extend the RSH relation to the temporal domain and test its validity along the trajectories of fluid tracers and of inertial particles whose density is smaller/larger than the fluid one while their sizes span the interval from the dissipative to the inertial range of scales. The manuscript is organized as follows: First we gives details on the numerical methods of the

DNS. We then present the extension of RSH to the Lagrangian domain and we test it on the trajectories of fluid tracers. In the last section we investigate the case of inertial particles: we show under which conditions the Lagrangian RSH still holds and how it should be modified in the special case of highly-inertial particles.

II. NUMERICAL METHODS

The incompressible fluid velocity $\mathbf{u}(\mathbf{x}, t)$, $\nabla \cdot \mathbf{u} = 0$, evolves according to the Navier-Stokes equations :

$$\frac{D\mathbf{u}}{Dt} \equiv \frac{\partial \mathbf{u}}{\partial t} + \mathbf{u} \cdot \nabla \mathbf{u} = -\frac{\nabla p}{\rho_f} + \nu \Delta \mathbf{u} + \mathbf{f}, \quad (2)$$

where p denotes the pressure, ρ_f the fluid density assumed constant, and \mathbf{f} an external large-scale forcing injecting energy at a mean rate $\langle \varepsilon \rangle = \langle \mathbf{u} \cdot \mathbf{f} \rangle$. Together with the Eulerian field we integrated the Lagrangian evolution of fluid tracers: $d\mathbf{x}(t)/dt = \mathbf{v} \equiv \mathbf{u}(\mathbf{x}(t), t)$, and point-particles by means of a model of dilute suspensions of small passively advected spherical particles, as derived in Refs. [11, 12, 13]:

$$\frac{d\mathbf{x}}{dt} = \mathbf{v}, \quad \frac{d\mathbf{v}}{dt} = \beta \frac{D\mathbf{u}}{Dt} + \frac{1}{\tau_p}(\mathbf{u} - \mathbf{v}), \quad (3)$$

where \mathbf{x} and \mathbf{v} denote the particle position and velocity, respectively. In Eq. (3) the coefficient $\beta = 3\rho_f/(\rho_f + 2\rho_p)$ is related to the ratio between the density of the particle (ρ_p) and of the fluid (ρ_f); $\tau_p = a^2/(3\beta\nu)$ is the Stokes response time, with a the particle-radius. The Stokes number of the particle is defined as $St = \tau_p/\tau_\eta$, where $\tau_\eta \equiv (\nu/\langle \varepsilon \rangle)^{-1/2}$ is the dissipative time-scale of the turbulent flow. In our simulation the parameters β and St can be varied independently, therefore it is possible to consider also the case ($\beta = 0, St > 0$), corresponding to the limit to very heavy particles for which the fluid added mass is negligible while Stokes drag is the only relevant dynamical force. On the other hand the situation ($\beta = 1, St = 0$) is equivalent to the case of a perfect fluid tracer.

Eq. (2) is numerically integrated by means of a standard internally 2/3 de-aliased pseudo-spectral algorithm with a second order Adams-Bashforth time-advancing scheme. The very same time-scheme is used to track the particles evolving according to eq. (3): the time-step size in both cases is $O(10^{-2}\tau_\eta)$, however particle informations are recorded for post-processing/analysis at a rate of $10^{-1}\tau_\eta$. Interpolations of the velocity field, acceleration field (necessary for (3)) and velocity gradients at the particle positions, are done via a tri-linear algorithm. For a validation of our numerical method we address Ref. [14], where a satisfactory comparison on acceleration lagrangian statistics has been performed against an independent numerical implementation with several different features (field interpolation based on tri-cubic

scheme, external dealiasing procedure, a slightly different large scale forcing). In our DNS energy is injected at large-scale by maintaining the spectral content of the first two shells in Fourier space constant. Here we will report data coming from two sets of simulations with $N^3 = 2048^3$ and $N^3 = 512^3$ collocation points, corresponding to $Re_\lambda = 400$ and 180 , respectively, and sampling the parameter space $\beta \in [0 : 3]$, $St \in [0 : 4]$ with 64 (β, St) particles types. A total amount of $\sim 10^8$ particles are tracked in time. Results on the clustering of these particles in the turbulence have already been reported in Ref. [8, 9]. Inertia requires some time before particles reach their fractal (or multifractal) statistically stationary distributions [15, 16]. We therefore waited till the Lagrangian statistics became stationary (approximately one large-eddy turnover-time) before performing the analysis presented here. Measurements of velocity differences and gradients are based on sets of $O(10^6 - 10^7)$ particles which have been followed in time for few $O(1)$ large-eddy-turnover times.

III. REFINED SIMILARITY HYPOTHESIS IN THE LAGRANGIAN FRAME

A. Inertia effect on the statistics of principal invariants of velocity gradient tensor

We have already noted that the effects of inertia may be of particular interest for the present study. Inertial particles are not distributed homogeneously in the volume, centrifugal force tends to concentrate light particle inside strong elliptical regions, with high vorticity [7, 8, 17]; and heavy particle in hyperbolic regions, typical of intense shear. Following Chong et al. [18], the flow topology may be locally defined in terms of the two principal invariants of the velocity gradient tensor $\mathcal{A} = A_{ij} = \partial_i u_j$, namely $Q = -Tr[\mathcal{A}^2]/2$ and $R = -Tr[\mathcal{A}^3]/3$, (see also [19] for a recent study). Q represents the difference between a rotation-dominated and a dissipation-dominated flow topology, e.g., it is positive in a vortex core, while negative in a region characterized by high strain. The second parameter, R , analogously represents the competition between the vorticity production and the dissipation production. Also, the separatrix curve $(R/2)^2 + (Q/3)^3 = 0$ (so called Vieillefosse line [20]) discriminate between three real or one real and two complex-conjugate eigenvalues for \mathcal{A} , again meaning only-strain or vortical regions. In fig. 1 we show the joint probability density function $\mathcal{P}(Q, R)$ for different particle types as measured in the simulations at $Re_\lambda = 180$. The most striking effect is for light particles ($\beta = 3$), contrary to tracers and heavy particles ($\beta = 0$) they spend essentially all of their time in upper half-plane $Q > 0$, meaning that they constantly trapped in vortical regions.

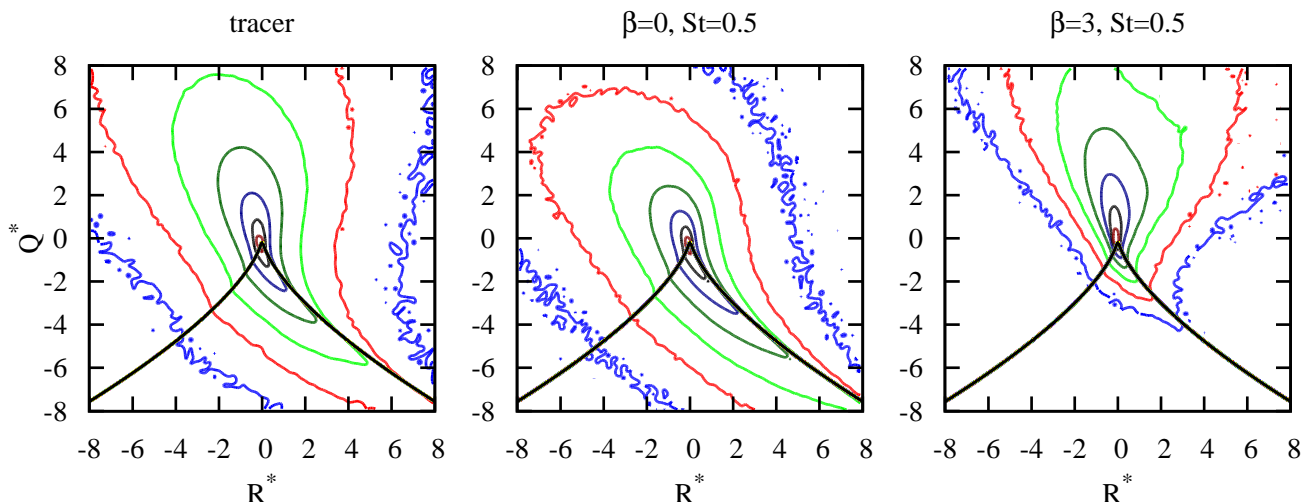


FIG. 1: Joint probability density function $\mathcal{P}(Q^*, R^*)$ of $Q^* \equiv Q/\langle Q^2 \rangle^{1/2}$ and $R^* \equiv R/\langle Q^2 \rangle^{3/4}$, for particles of different types. Contour lines are drawn at values 10^{-z} with $z = 0, 1, 2, 3, 4, 5, 6$ (from the center to the outside of the figure). The thick line traces the curve: $(R/2)^2 + (Q/3)^3 = 0$ (Viellefosse line), discriminating between complex (above) and real (below) eigenvalues of \mathcal{A} . Data come from $Re_\lambda = 180$ calculations.

B. Time correlation of symmetric and antisymmetric component of velocity gradient tensor

One also expects pretty different temporal correlations between particle trajectories and the underlying topology of the carrier flow. We look now at the symmetric/antisymmetric component of the velocity gradient tensor \mathcal{A} , because of their direct link with energy dissipation and enstrophy, [21, 22, 23]. We show in Fig. (2) the autocorrelation function of enstrophy, $\Omega = \frac{\nu}{2}(\mathcal{A} - \mathcal{A}^T)^2 = \frac{\nu}{2} \sum_{i,j} (\partial_i u_j - \partial_j u_i)^2$ and energy dissipation, $\epsilon = \frac{\nu}{2}(\mathcal{A} + \mathcal{A}^T)^2 = \frac{\nu}{2} \sum_{i,j} (\partial_i u_j + \partial_j u_i)^2$, along the particle trajectories for different values of inertia. As one can see both these quantities have short autocorrelation time, at $Re_\lambda = 180$ we find $T_\Omega = \int_0^\infty C_\Omega(\tau) d\tau \simeq 7\tau_\eta$ and similarly $T_\epsilon \simeq 5\tau_\eta$. However, the autocorrelation of enstrophy turns out to be rather sensitive to the type of particles, while energy dissipation is probed more or less uniformly. This is a clear indication that due to inertia, particle tends to leave in regions with very different vorticity contents, while energy dissipation - although different in intensity - turns out to be a more robust quantity in term of coherence-in-time: This result will be very useful in our following discussion.

C. RSH and its generalized formulation

Along the trajectory of a fluid tracer $\mathbf{x}(t)$ the velocity difference will be denoted as $\delta_\tau v = v(t + \tau) - v(t)$ and similarly we define a coarse grained energy dissipation measured along the trajectory as $\epsilon_\tau = \int_t^{t+\tau} \epsilon(\mathbf{x}(t), t) dt$ (see also [24]). The RSH (1) can be translated from space to time by making the assumptions that $\delta_\tau v \sim \delta_r u$ and $\epsilon_\tau \sim \epsilon_r$ when τ and r are linked through the eddy turnover

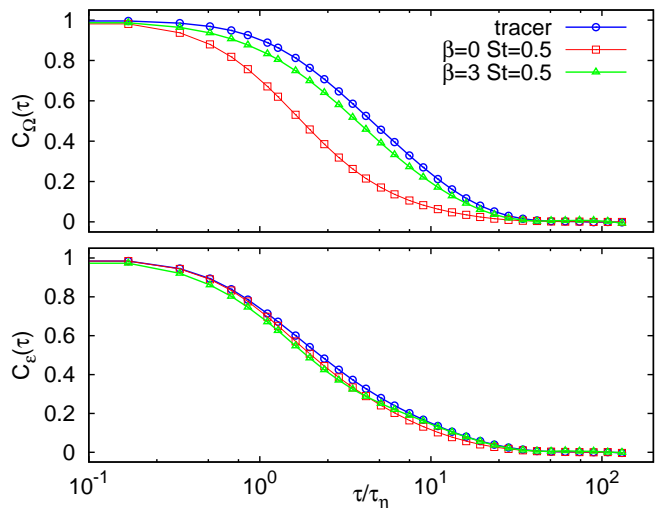


FIG. 2: Temporal autocorrelation function, i.e., $C_X(\tau) \equiv \langle X'(t) - X'(t + \tau) \rangle / \langle X'^2 \rangle$ with $X'(t) = X(t) - \langle X \rangle$, of the enstrophy $X = \Omega$ (top) and the energy-dissipation-rate $X = \epsilon$ (bottom) for fluid tracers and for inertial particles with $St = 0.5$, $\beta = 0, 3$, at $Re_\lambda = 180$.

time definition, $\tau(r) \sim r/\delta_r u$. This argument leads to the Lagrangian refined similarity hypothesis (LRSH):

$$\delta_\tau v \sim \tau^{1/2} \epsilon_\tau^{1/2}. \quad (4)$$

In order to test Eq. (4) one should verify, for any exponent p , the scaling relations:

$$\langle (\delta_\tau v)^p \rangle \simeq \tau^{p/2} \langle \epsilon_\tau^{p/2} \rangle, \quad (5)$$

where \simeq means equal apart from a multiplicative constant depending only on p , in the inertial range. In the

time domain the inertial range is defined as the interval, $\tau_\eta \ll \tau \ll T_L$, where T_L is the Lagrangian integral time scale, which is estimated as the autocorrelation time of velocity of fluid tracers, i.e., $T_L = \int_0^\infty C_v(\tau) d\tau$, with $C_v(\tau) \equiv \langle v(t)v(t+\tau) \rangle / \langle v^2 \rangle$. As one can estimate $T_L/\tau_\eta \sim Re_\lambda$, the extension of the inertial range in dissipative time-scale units extends over roughly two decades in the present numerical study.

In contrast to the 4/5-law (consequence of the Karman-Howarth equation) leading to exact scaling properties for third order velocity increments in the Eulerian frame, we do not have any exact scaling relation derivable from NS equations in the Lagrangian domain. Furthermore, it is known that in the Lagrangian frame, finite Reynolds effects induce larger deviations from a power law regime than what observed in Eulerian frame [25]. To overcome these effects, following [26], we can generalize the above expression (5) by using its Extended Self Similarity (ESS) form, namely:

$$\langle (\delta_\tau v)^p \rangle \simeq \left(\frac{\langle (\delta_\tau v)^2 \rangle}{\langle \varepsilon_\tau \rangle} \right)^{p/2} \langle \varepsilon_\tau^{p/2} \rangle \quad (6)$$

D. Numerical tests of LRSB

In Figure 3(a) we present a test of Eq. (5) for $p = 4$ for particles with $\beta = 1$, $St = 0$, i.e. fluid tracers (circles) and very-heavy particles with $\beta = 0$, $St = 2$ (triangles). In Figure 3(b), we show instead the relation from Eq. (6) for the same particle types. Two major results emerge. First the LRSB, as expressed by Eq. (6) is well verified for the transport of particles in turbulent flows. The use of the ESS version for LRSB is able to overcome finite size/time effects which are usually observed at relatively low Reynolds number (see [25]). The second important result, which will be investigated later on in this manuscript, comes from inspecting the validity of (6) for different Stokes numbers. Equation (6) is supposed to be valid both in the inertial range and in the dissipative range (where the velocity field is smooth) though with different offset. This is clearly observed in Figure 3(b) for the case $St = 0$. It is already known that by increasing the Stokes number, particles tends to escape from strong vorticity region, thus decreasing the effect of the dip present in between dissipative and inertial scales [27]. As a consequence, for $St = 2$ we observe almost no deviation of Eq. (6) in the range of scales between the inertial and the dissipative ranges.

To have a more quantitative check, we look now at the ratio between the two sides of Eq. (6), namely at $\langle (\delta_\tau v)^p \rangle$ divided by $\langle \varepsilon_\tau^{p/2} \rangle \langle (\delta_\tau v)^2 \rangle^{p/2} \langle \varepsilon_\tau \rangle^{-p/2}$, as a function of the time difference τ . In Figure 4 we show its behavior for the order $p = 4$ fluid tracers particles, the time difference τ is normalized by the dissipative time-scale τ_η . We observe a plateau (see circles symbols, in Fig 4) for $\tau/\tau_\eta \geq 5$. Notice that also in the dissipative range the compensation

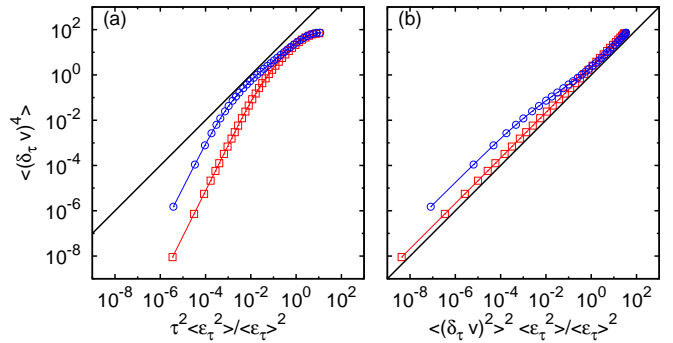


FIG. 3: Test of LRSB along the trajectories of tracers and heavy particles at $Re_\lambda = 400$. (a) For $p = 4$ we show Eq. (5) for $St = 0$ (circles) and $St = 2$ (squares). (b) We show the validity of Eq. (6) for the same values of p and St . Straight lines correspond to the theoretical scaling prediction. Data come from $Re_\lambda = 400$ calculations.

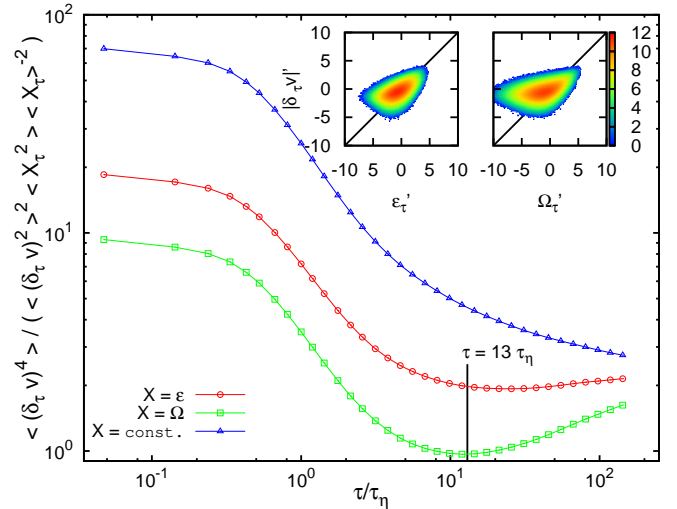


FIG. 4: Test of LRSB along the trajectories of tracers ($Re_\lambda = 400$). It is plotted $\langle (\delta_\tau v)^4 \rangle / (\langle (\delta_\tau v)^2 \rangle^2 \langle X_\tau^2 \rangle \langle X_\tau \rangle^{-2})$: (circles) represent the case $X = \varepsilon$, (squares) the case $X = \Omega$, and (triangles) the case $X = \text{const.}$ In the inset the joint pdf: $P(\varepsilon'_\tau, |\delta_\tau v|)$ and $P(\Omega'_\tau, |\delta_\tau v|)$ at $\tau = 13\tau_\eta$; (note that the prime symbol denotes variables normalized respect to their mean values, i.e. $x' \equiv x/\langle x \rangle$).

works well, as it should from the requirement that the velocity field becomes differentiable, $\delta_\tau v \sim \tau$. However, the plotted ratio shows a mismatch with the value attained in the inertial range. The transition between the two plateaux occurs around the dissipative time scale, where the presence of vortex trapping has been shown to spoil the scaling behavior of Lagrangian structure functions $\langle (\delta_\tau v)^p \rangle$ of the tracers [28, 29, 30, 31]. In the same figure we show that using the coarse grained enstrophy, i.e., Ω_τ instead of ε_τ , the compensation is worse (squares). Similarly, compensation with enstrophy does not work neither for heavy nor for light particles (not shown). Compensating without coarse grained quantities, i.e. checking

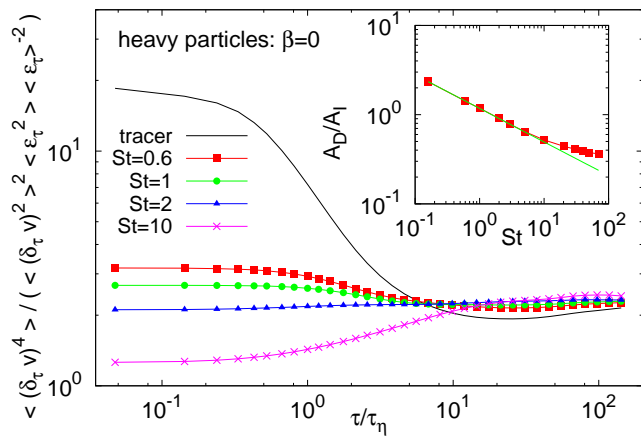


FIG. 5: Same as in Fig.4, here also along the trajectories of heavy particles ($\text{Re}_\lambda = 400$). It is plotted $\langle (\delta_\tau v)^4 \rangle \langle \varepsilon_\tau \rangle^2 / (\langle \varepsilon_\tau^2 \rangle \langle (\delta_\tau v)^2 \rangle^2)$. Particles with $St = 0.6, 1, 2, 10$ are compared with the result for tracers (solid black line). The LRSH is satisfied both in the inertial and in the dissipative ranges. The prefactors, A_I and A_D , however differs in the two regions. Notice that for the largest Stokes, $St = 10$, the smallest time lags where LRSH is verified, as expected, roughly $\tau \sim 10\tau_\eta$. In the inset, the behavior of ratio of prefactors A_D/A_I is plotted vs. St . For small St values a behavior as $St^{-0.38}$ is found (solid line in the inset).

the deviation from dimensional, non-intermittent, scaling does not provide a good plateau (triangles in Fig 4). This result supports the validity of LRSH only when using the energy dissipation as the main driving process along the particle motion. The behavior for intense fluctuations (moments higher than $p = 6$) can not be checked quantitatively due to the lack of statistics. Nevertheless, in the same figure, we show the joint probability density functions, $\mathcal{P}(\Omega_\tau, |\delta_\tau v|)$ and $\mathcal{P}(\varepsilon_\tau, |\delta_\tau v|)$, for a time lag $\tau = 13 \tau_\eta$. Velocity increments are more correlated with coarse-grained energy than with enstrophy, as shown by the high probability measured for simultaneous intense values of $|\delta_\tau v|$ and ε_τ .

Having established the validity of the LRSH, we strive now at investigating the effect of different Stokes number and different density properties.

IV. LRSH IN THE (β, St) PARTICLE PARAMETER SPACE

A. Heavy particles ($\beta = 0$) at $St \sim O(1)$

When particles have inertia their trajectories deviate from material lines of the flow. In principle, one expects that for very small value of the inertia (particles very close to fluid tracers) no appreciable discrepancies can be measured. In Figure 5 it is shown the test for the LRSH compensated with the energy dissipation rate. From One can appreciate that in the inertial range, e.g. $\tau/\tau_\eta \geq 5$ the LRSH is well verified for all the Stokes considered. In

the dissipative range it is also verified but with a different proportionality constant. In particular, the important mismatch observed between the two plateaus for tracers in (Fig.4) here is reduced considerable as soon as some inertia is switched on. This confirms that heavy particles are quickly expelled out of vortex filaments, and therefore much less sensitive to the transition around $\tau/\tau_\eta \sim 1$ than tracers [27] (the opposite will happen for light particles, see below).

The behavior of the ratio (A_D/A_I) of the plateaus displayed by $\langle (\delta_\tau v)^4 \rangle \langle \varepsilon_\tau \rangle^2 / (\langle \varepsilon_\tau^2 \rangle \langle (\delta_\tau v)^2 \rangle^2)$ respectively in the dissipative range (A_D for $\tau \ll \tau_\eta$) and in the inertial range (A_I for $\tau \leq 10\tau_\eta$), is shown in the inset of Fig. 5. The estimate for the slope of A_D/A_I vs. St can be provided by the following reasoning. First we notice that the inertial constant A_I is almost insensitive from the Stokes value, therefore the dissipative constant A_D carries all the St dependency. Moreover, we have measured that the single point energy dissipation statistics is pretty insensitive to the Stokes number (see again fig. 2). As a consequence the main dependency on St for the ratio A_D/A_I comes from the flatness factor $F(\tau) \equiv \langle (\delta_\tau v)^4 \rangle / \langle (\delta_\tau v)^2 \rangle^2$ in the intermediate-dissipative τ limit. It is reasonable to estimate the difference between $F(\tau)$ at changing Stokes, but fixed Reynolds, as given by the value of the flatness at the particle response time: $F(\tau_p) \sim St^{\zeta_4 - 2\zeta_2}$, where ζ_p is the p -th order scaling exponent for Lagrangian structure functions $\langle (\delta_\tau v)^p \rangle \sim \tau^{\zeta_p}$. Based on the experimental values $\zeta_4 \simeq 1.6$ and $\zeta_2 \simeq 1$ [30], this estimate gives $A_D/A_I \sim St^{-0.4}$, not too far from the fit $St^{-0.38 \pm 0.05}$ to our numerical data, see inset of Fig 5.

B. Finite density contrast: heavy and light particles

We now look at the statistical properties of particles with finite density contrast, i.e. also $\beta \neq 0$. In Figure 6 it is shown, for $St = 1$, the behavior of the compensated tests for LRSH for different values of β spanning the full range $[0 : 3]$. In the inset it is also shown the behavior, this time as function of β , of the A_D/A_I ratio. Notice how the critical value $\beta = 1$, discriminating between heavy ($\beta < 1$) and light ($\beta > 1$) particles plays a crucial role. Again LRSH is well verified in the inertial range, but the change to a different plateau around $\tau/\tau_\eta \sim 1$ is now much more abrupt when light particles are considered: for those the vortex trapping is more pronounced, as all light particles quickly move towards high vorticity regions, showing a very sensitive dependency around the dissipative time dynamics. A model for the dependency of A_D/A_I vs. β is presently not available.

C. Heavy particles ($\beta = 0$) with large inertia

Having studied the case of particles with small inertia, we now focus on the case of extreme inertia, i.e., when

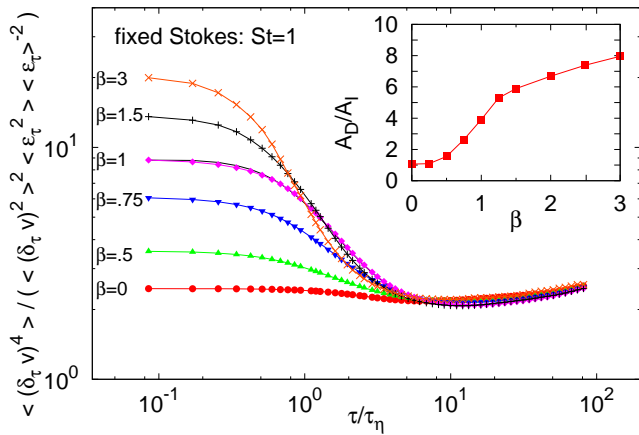


FIG. 6: Same as in fig. 4 along the trajectories of heavy/light inertial particles with $St = 1.0$ ($Re_\lambda = 180$). It is plotted $\langle (\delta_\tau v)^4 \rangle \langle \varepsilon_\tau \rangle^2 / (\langle \varepsilon_\tau \rangle^2 \langle (\delta_\tau v)^2 \rangle^2)$. Particles with $\beta = 0, 0.5, 0.75, 1.0, 1.5, 3.0$ are compared with the result for tracers (solid black line). The LRSH is satisfied both in the inertial and in the dissipative ranges. As for the case of heavy particles the prefactors differs in the two regions. In the inset, the behavior of ratio of prefactors A_D/A_I is plotted vs. β .

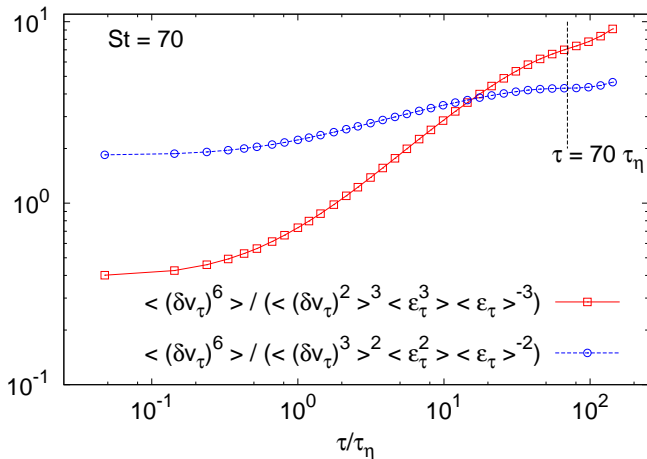


FIG. 7: Particles with very large inertia do not verify the LRSH (6), but follow the Eulerian version (7). We show this for the order $p = 6$ on particle trajectories with $St = 70$, at $Re_\lambda = 400$. As it can be seen, in the inertial range, the Eulerian RSH compensate better than LRSH.

the response time of the particle is at the top end of the inertial time-range, or $St \sim O(10)$. In this condition, for time lags $\tau < \tau_p$ when the particle filters out most of the underlying turbulent fluid fluctuations and evolves nearly ballistically, one can predict a different behavior for $\delta_\tau v$. Along the trajectory of a ballistic particle, the relation linking scale to time is $\tau(r) \simeq r/v_0$ where the typical particle velocity v_0 is proportional to root mean square fluid velocity. Recasting eq.(1) from space to time notation we obtain again an Eulerian-like RSH relation,

$$(\delta_\tau v) \sim (\tau/v_0)^{1/3} \varepsilon_\tau^{1/3}, \text{ or:}$$

$$\langle (\delta_\tau v)^p \rangle \simeq \left(\frac{\tau}{v_0} \right)^{p/3} \langle \varepsilon_\tau^{p/3} \rangle \quad (7)$$

The generalized version of (7) reads now

$$\langle (\delta_\tau v)^p \rangle \simeq \frac{\langle \varepsilon_\tau^{p/3} \rangle}{\langle \varepsilon_\tau \rangle^{p/3}} \langle (\delta_\tau v)^3 \rangle^{p/3} \quad (8)$$

In Figure 7 we present a test of this idea for $\langle (\delta_\tau v)^p \rangle$ with $p = 6$: For particles with very large Stokes numbers ($St = 70$) we compensate the velocity increments both with respect to the prediction of the Lagrangian RSH and with respect to the prediction of the Eulerian RSH in its generalized version. The compensation with the Eulerian RSH works appreciably better in the range $\tau \leq St \cdot \tau_\eta$ than the compensation with LRSH.

V. CONCLUSIONS

In summary, some important statistical properties of velocity gradients along trajectories of fluid tracers, heavy and light particles have been investigated. We used high-resolution, high-statistic numerical data to correlate the temporal properties of velocity gradients and velocity differences along trajectories. We demonstrated that the Refined Similarity Hypothesis is well verified both for fluid particles and particles with response time in the dissipative regime, a feature that we dubbed Lagrangian RSH. Around the dissipative time lags, heavy and light particles behave strongly differently, due to the effect of being expelled/concentrated out/in vortex filaments. The dynamics at those time lags becomes markedly dependent on the underlying topological flow properties.

Understanding the RSH in the Lagrangian domain may also have important applied consequences. In many applications, the geometry of the system and/or the intensity of turbulence do not allow for a direct attack of the problem using numerical simulations of the Navier-Stokes equations. Modeling is needed for both the underlying fluid and for the particle equations. Typically, the ideal model, would like to replace Eqs.(3)-(2) with a Langevin-like equation for the particle evolution [32, 33]: $d\mathbf{x}/dt = \mathbf{v}$, $d\mathbf{v}/dt = \mathcal{D}(\mathcal{A})\mathbf{v} + \mathbf{\Gamma}(t)$ where the $\mathbf{\Gamma}$ represents some stochastic noise induced by the underlying turbulent fluctuations. The hard physical problem is in the modelization of the drift term, $\mathcal{D}(\mathcal{A})$, depending on the local gradient structure along the trajectories (see [34, 35, 36] for recent attempts). Such term should also take into account effects induced by preferential concentration in/out vortex filaments for the case of inertial particles around the dissipative time lags.

The numerical database presented here can play a crucial role for benchmarking stochastic models for tracers and inertial particles in turbulence. Data from this study are publicly available in unprocessed raw format from the iCFDdatabase (<http://cfd.cineca.it>).

During the preparation of this manuscript we got aware of a slightly similar investigation [37] where Lagrangian correlation of velocity and pressure gradients are studied conditioning on the initial Eulerian energy dissipation, a sort of mixed Eulerian-Lagrangian refined Kolmogorov hypothesis, different from the fully Lagrangian view point adopted here.

We thank J. Bec, M. Cencini and A. S. Lanotte for several discussions. DEISA Consortium (co-funded by the EU, FP6 project 508830) is acknowledged for support within the DEISA Extreme Computing Initiative (www.deisa.org). LB acknowledges partial support from CNISM. EC acknowledges support from CNRS and Agence Nationale de la Recherche.

-
- [1] U. Frisch, *Turbulence: The Legacy of A. N. Kolmogorov* (Cambridge University Press, Cambridge, 1995).
 - [2] A. N. Kolmogorov, *J. Fluid Mech.* **13**, 82 (1962).
 - [3] A. Oboukhov, *J. Fluid Mech.* **13**, 77 (1962).
 - [4] G. Stolovitzky and K. R. Sreenivasan, *Rev. Mod. Phys.* **66**, 229 (1994).
 - [5] S. Chen, K. R. Sreenivasan, M. Nelkin, and N. Cao, *Phys. Rev. Lett.* **79**, 2253 (1997).
 - [6] F. Toschi, E. Leveque, and G. Ruiz-Chavarria, *Phys. Rev. Lett.* **85**, 1436 (2000).
 - [7] J. K. Eaton and J. R. Fessler, *Int. J. Multiphase Flow* **20**, 169 (1994).
 - [8] E. Calzavarini, M. Kerscher, D. Lohse, and F. Toschi, *J. Fluid Mech.* **607**, 13 (2008).
 - [9] E. Calzavarini, M. Cencini, D. Lohse, and F. Toschi, *Phys. Rev. Lett.* **101**, 084504 (2008).
 - [10] T. Toschi and E. Bodenschatz, *Annu. Rev. Fluid Mech.* **41**, 375 (2009).
 - [11] M. R. Maxey and J. J. Riley, *Phys. Fluids* **26**, 883 (1983).
 - [12] R. Gatignol, *J. Mec. Theorique et Appliquée* **1**, 143 (1983).
 - [13] T. Auton, J. Hunt, and M. Prud'homme, *J. Fluid Mech.* **197**, 241 (1988).
 - [14] E. Calzavarini, R. Volk, M. Bourgoïn, E. Lévêque, J.-F. Pinton, and F. Toschi, *Springer Proc. Phys.* **132**, 11 (2009).
 - [15] J. Bec, *Phys. Fluids* **15**, L81 (2003).
 - [16] J. Bec, *J. Fluid Mech.* **528**, 255 (2005).
 - [17] M. Maxey, *J. Fluid Mech.* **174**, 441 (1987).
 - [18] M. S. Chong, A. E. Perry, and B. J. Cantwell, *Phys. Fluids A* **2**, 765 (1990).
 - [19] B. Luethi, M. Holzner, and A. Tsinober, *J. Fluid Mech.* p. (in press) (2009).
 - [20] P. Vieillefosse, *Physica A* **125**, 150 (1984).
 - [21] P. K. Yeung, S. B. Pope, E. A. Kurth, and A. G. Lamorgese, *J. Fluid Mech.* **582**, 399 (2007).
 - [22] B. Lüthi, A. Tsinober, and W. Kinzelbach, *J. Fluid Mech.* **528**, 87 (2005).
 - [23] M. Guala, A. Liberzon, A. Tsinober, and W. Kinzelbach, *J. Fluid Mech.* **574**, 405 (2007).
 - [24] M. S. Borgas, *Phil. Trans.: Physical Sciences and Engineering* **342**, 379 (1993).
 - [25] P. K. Yeung, *Annu. Rev. Fluid Mech.* **34**, 115 (2002).
 - [26] R. Benzi, L. Biferale, S. Ciliberto, M. Struglia, and R. Tripiccone, *Physica D* **96**, 162 (1996).
 - [27] J. Bec, L. Biferale, M. Cencini, A. S. Lanotte, and F. Toschi, *Phys. Fluids* **18**, 081702 (2006).
 - [28] I. Mazzitelli and D. Lohse, *New J. Phys.* **6**, 203 (2004).
 - [29] L. Biferale, G. Boffetta, A. Celani, A. Lanotte, and F. Toschi, *Phys. Fluids* **17**, 021701 (2005).
 - [30] L. Biferale, E. Bodenschatz, M. Cencini, A. Lanotte, N. Ouellette, F. Toschi, and H. Xu., *Phys. Fluids* **20**, 065103 (2008).
 - [31] A. Arnéodo, R. Benzi, J. Berg, L. Biferale, E. Bodenschatz, A. Busse, E. Calzavarini, B. Castaing, M. Cencini, L. Chevillard, et al., *Phys. Rev. Lett.* **100**, 254504 (2008).
 - [32] S. B. Pope, *Turbulent Flows* (Cambridge University Press, Cambridge, 2000).
 - [33] B. L. Sawford and F. M. Guest, *Boundary-Layer Meteorology* **54**, 147 (1991).
 - [34] A. Naso and A. Pumir, *Phys. Rev. E* **72**, 056318 (2005).
 - [35] L. Chevillard and C. Meneveau, *Phys. Rev. Lett.* **97**, 174501 (2006).
 - [36] L. Biferale, L. Chevillard, C. Meneveau, and F. Toschi, *Phys. Rev. Lett.* **98**, 214501 (2007).
 - [37] H. Yu and C. Meneveau, private communication (2009).